Probing the production mechanism of neutron-rich nuclei in multinucleon transfer reactions

Xiang Jiang and Nan Wang*
College of Physics and Optoelectronic Engineering, Shenzhen University, Shenzhen 518060, China

(Received 2 July 2019; published 9 January 2020)

Aiming at understanding the production mechanism of new neutron-rich nuclei around $N = 126$, the multinucleon transfer reaction ^{136}Xe + ^{208}Pb at $E_{\mathrm{c.m.}} = 450$ MeV has been investigated in the framework of the three-dimensional time-dependent Hartree-Fock (TDHF) theory and a statistical model GEMINI. The calculated production cross sections of the targetlike fragments are compared with the experimental data. The model predictions can well describe the yields of nuclei near the target. The reactions of ^{132}Sn + ^{208}Pb at different incident energies above the Coulomb barrier are also studied. It is shown that this system is a better candidate for producing $N = 126$ neutron-rich nuclei than using ^{136}Xe as the projectile because of the favored proton pickup and neutron stripping transfer channels. The study of de-excitation effect indicates that the suitable incident energy to synthesize neutron-rich nuclei should be just above the Coulomb barrier. It is also found in ^{132}Sn + ^{208}Pb that about 50 new neutron-rich nuclei with the production cross sections larger than 10^{-6} mb are obtained dominantly through quasifission and deep-inelastic collisions. However, those with $N = 126$ are mainly from grazing collisions. Comparison with the results of the GRAZING model is also discussed.

DOI: 10.1103/PhysRevC.101.014604

I. INTRODUCTION

Multinucleon transfer (MNT) between massive nuclei takes place in reactions at energies in the vicinity of the Coulomb barrier and up to intermediate energies around the Fermi energy domain, from peripheral quasielastic scattering to more central deep-inelastic collisions. These experiments have been widely studied in the past four decades [1–6] to extract information on nucleon-nucleon correlations, nuclear structure, reaction mechanisms, nucleon transfer modes, and so on. Recently, such reactions have gained renewed interest and are actively discussed as possibilities to populate new exotic nuclei, especially the neutron-rich ones which can be provided as beams to synthesize extreme neutron-rich nuclei close to the neutron drip line and superheavy nuclei located at the island of stability. This is one of the aims of the upcoming radioactive ion beam facilities. Those nuclei are also important in nuclear astrophysics investigations. For instance, neutron-rich nuclei around the $N = 126$ neutron shell closure, the last waiting point along the r-process [7], can provide information on the observed peak structure around $A \approx 195$ in the solar r-abundance distribution [8].

Inspired by the predictions of Zagrebaev and Greiner [9–11], many experiments have been carried out all around the world to synthesize new neutron-rich nuclei. ^{48}Ca + ^{238}U and ^{48}Ca + ^{248}Cm were performed at Helmholtz Centre for Heavy Ion Research (GSI) for synthesizing new neutron-rich nuclei in the transuranium region [12,13]. Reactions of ^{64}Ni, ^{136}Xe bombarding on nuclei in the Pb region around the Coulomb barrier were performed at Dubna [14], Argonne [15], and GSI [16] to produce new neutron-rich nuclei with $N = 126$, but no new isotopes were detected. In 2015, ^{136}Xe + ^{198}Pt at the incident energy of 8 MeV/nucleon (about 55% higher than the Coulomb barrier) was carried out at Grand Accélérateur National d'Ions Lourds (GANIL) [8]. The results show remarkable improvement of the production cross sections of the neutron-rich $N = 126$ nuclei with $Z \leqslant 78$, compared with the results of fragmentations. This verifies that the MNT reactions would be an optimum route to synthesize neutron-rich nuclei around $N = 126$.

Recently, many theoretical models have been developed on different bases for understanding the complex transfer process. For example, semiclassical models like GRAZING [17,18] and the complex Wentzel-Kramers-Brillouin (CWKB) [19] have been widely and successfully used to describe few-nucleon transfer at grazing impact parameters [20–26]. The dinuclear system (DNS) model [27–33] and the improved quantum molecular dynamics (ImQMD) model [34–36] also show success in reproducing the measurements of MNT reactions. We also notice that Karpov recently developed a multidimensional dynamical model of nucleus-nucleus collisions based on the Langevin equations and by using this model the experimental results of some MNT reactions can be well reproduced [37]. However, there are empirical parameters in these models. It is clear that transfer processes in different impact parameter regions are governed by different mechanisms including quasifission, deep inelastic, and quasi elastic. Moreover, nuclear structure and quantum effects play significant roles in low-energy reactions.

In order to investigate the production mechanism of neutron-rich nuclei in MNT reactions in a unified way in nucleonic degrees of freedom quantally and without adjustable parameters, in this work the MNT reactions are studied in the TDHF theory [38,39]. TDHF can describe low-energy

*Corresponding author: wangnan@szu.edu.cn

heavy-ion collisions microscopically and provide insight about the average behavior of the collision dynamics. Density rearrangement, particle transfer, neck formation, and other dynamical effects are all included self-consistently. The present TDHF calculations are performed in three-dimensional (3D) space with more accurate numerical methods and without any symmetry restrictions. Modern Skyrme parametrizations with all time-odd terms are also available. The 3D TDHF investigations have been widely used for many subjects, for instance, collective vibration [40–42], fusion reaction [43–46], fission dynamics [47–49], dissipation mechanism [50–54], transfer reaction [34,55–60], and so on. In order to compare the calculated results with the experimental data, the de-excitation of hot primary fragments which can considerably alter the isotopic distributions thus should be considered. Unfortunately, this process cannot be treated directly in TDHF or other dynamical models. It can be cured by using the state-of-art statistical code GEMINI++, an improved version of GEMINI written by Charity [61–64], which has been widely used to simulate the hot equilibrium source de-excitation, or as an "afterburner" code to analyze the hot fragment decay after dynamical simulation [65,66]. Such combinations of dynamical model like TDHF or ImQMD together with the statistical code have been widely used recently [36,55,58,59,67].

This paper is organized as follows. The outlines of the TDHF approach, particle number projection (PNP) method, and the numerical details are given in Sec. II. In Sec. III, numerical results are shown and compared with the experimental data. Finally, a summary is given in Sec. IV.

II. FORMALISM AND NUMERICAL DETAILS

TDHF is the time-dependent form of the static HF, and the equations can be derived from the variation of the action

$$S = \int dt \langle \Psi | i\partial_t - \hat{H} | \Psi \rangle, \tag{1}$$

with respect to the single-particle wave function ψ_α^* [68], where Ψ is the correlated many-body wave function of the system adopted as a Slater determinant, which is an antisymmetrized product of all single-particle wave functions. The single-particle Hamiltonian is related to Skyrme energy density functional (EDF) which depends on local densities.

The wave functions of the projectile and target will overlap during the collisions. Single-particle wave functions will partially exchanged between the reactants. Here, only binary fragments are obtained at the end of TDHF calculation since the Coulomb repulsion is too large for the system to fuse as a compound nucleus ($Z_P Z_T = 4428$ and 4100 for ^{136}Xe + ^{208}Pb and ^{132}Sn + ^{208}Pb, respectively). The expectation values of the charge and mass numbers for each fragment can be easily obtained. Since the outgoing states are superpositions

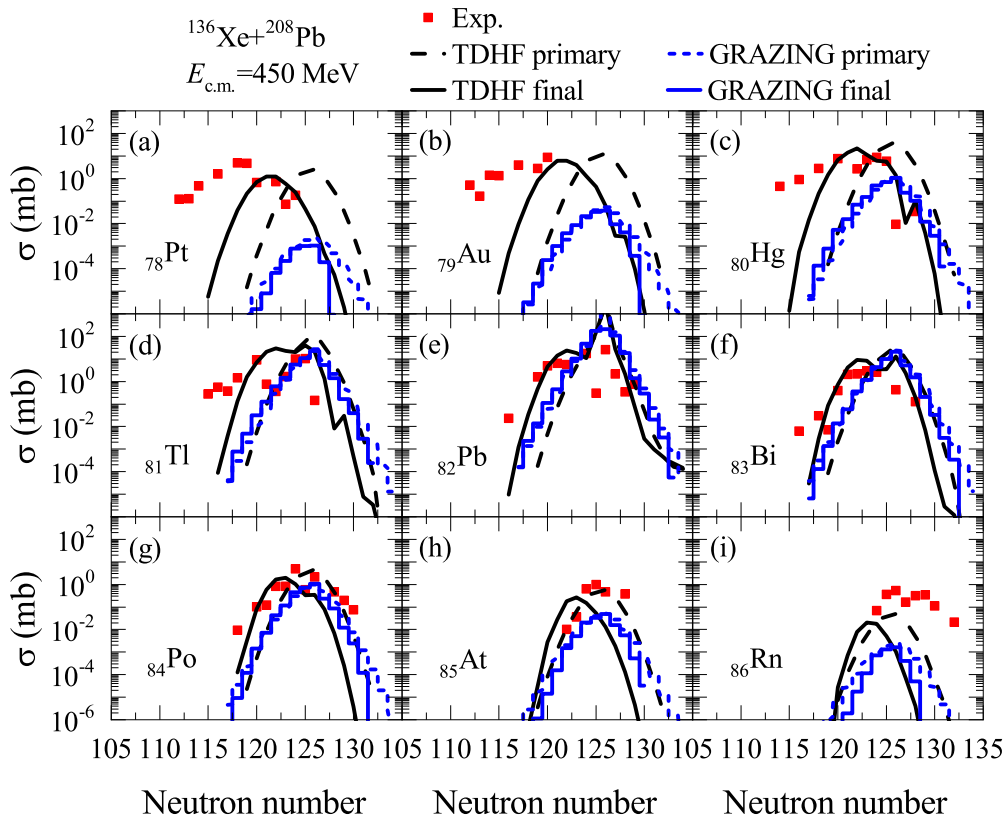

FIG. 1. Production cross sections of the TLFs in ^{136}Xe + ^{208}Pb at $E_{c.m.} = 450$ MeV. The solid squares represent the experimental data which are taken from Ref. [15]. The black dashed and solid lines are the predicted primary and final production cross sections of TDHF+GEMINI, respectively. Those of GRAZING are obtained from Ref. [78] with default parameters and presented by blue dashed and solid folding lines.

of different eigenstates of particle number operators, the expectation values are not "good" quantum numbers. This can be cured by the introducing PNP operator, which is [69,70]

$$\hat{P}_V(N) = \frac{1}{2\pi}\int_0^{2\pi} d\phi e^{i\phi(\hat{N}_V - N)}, \tag{2}$$

where the subscript V denotes the region of coordinate space encompassing one of the primary fragments (before GEMINI++ de-excitation), $\hat{N}_V = \sum_{\alpha=1}^{N^q} \Theta_V(\boldsymbol{r})$, and $\Theta_V(\boldsymbol{r}) = 1$ if $\boldsymbol{r} \in$ subspace V and 0 elsewhere.

The probability of finding N particles in subspace V is then obtained accordingly. The cross section of primary fragment with neutron number N and charge number Z at a certain incident energy is

$$\sigma_{N,Z} = 2\pi \int_{b_{\min}}^{b_{\max}} dbP_{N,Z}(b)b, \tag{3}$$

where $P_{N,Z} = P_N P_Z$; $b_{\min}$ is the critical impact parameter inside which fusion happens. Here, as we mentioned, the system cannot fuse at all. Thus, $b_{\min} = 0$ is adopted. $b_{\max}$ is a cutoff impact parameter which depends on the incident energy and it should be large enough to guarantee that most of the transfer cross sections are included.

Here the static and dynamical calculations are performed by using the code SKY3D [71] in a three-dimensional (3D) Cartesian box with Skyrme SLy6 parametrization which was developed with an emphasis on describing neutron-rich matter [72]. Note that the center-of-mass correction is omitted in TDHF calculations [71,73]. The lattice spacing is 1.0 fm in all three directions and the time step is $\triangle t = 0.2$ fm/c. The reactants are initially placed at a separation distance of 24 fm along the collision z axis and we assume that they approach each other asymptotically on a Coulomb trajectory. The impact parameter ranges from 0 to $b_{\max}$ with the interval $\Delta b = 1$ fm. For each impact parameter, the TDHF simulations are stopped when the separation distance of the primary fragments after collision reaches 30 fm and the wave functions are used to get the proton and neutron distributions. The integral over ϕ in Eq. (2) is performed with an M-point uniform discretion. Here $M = 300$ is adopted for convergence.

In order to investigate the de-excitation of the primary fragments, the code GEMINI++ with default parameters [64,74] is adopted. The charge and mass numbers, as well as the excitation energies and the angular momentum of one fragment, should be obtained as the inputs of the code. For a certain channel with N neutrons and Z protons in the target-like fragment (TLF), the excitation energy can be evaluated directly by using the projection method [57,58]. However, because of the huge computational cost for heavy systems, here we adopt a simpler method which gives quantitatively similar results to those of the projection method [58]. In this simpler method, the total excitation energy of the system can be obtained as $E^*_{\rm tot} = E_{\rm c.m.} - E_k + Q(N,Z)$, where E_k is the total kinetic energy and $Q(N,Z)$ denotes the ground-state Q value. The ground-state masses of projectile-like fragment (PLF) and TLF are adopted from AME2016 [75,76] and FRDM(2012) [77]. Actually, the Hartree-Fock ground-state masses of all possible PLF and TLF should be obtained for consistency, but it is time consuming and the masses depend on the Skyrme EDF. $E^*_{\rm tot}$ is then distributed in the primary fragments in proportion to their masses. Average angular momentum of the fragments can be directly obtained in TDHF. The de-excitation process of a certain TLF should be repeated $M_{\rm trial}$ times due to the statistical nature of GEMINI++. Here $M_{\rm trial} = 1000$ is used. The number of events in which final fragment (after GEMINI++ de-excitation) with $(N_{\rm final}, Z_{\rm final})$ is counted and denoted as $M(N_{\rm final}, Z_{\rm final})$. Then the final production cross section is given as

$$\sigma_{N_{\rm final},Z_{\rm final}} = 2\pi \int_{b_{\min}}^{b_{\max}} bdb \sum_{N\geqslant N_{\rm final}, Z\geqslant Z_{\rm final}} P_{N,Z}(b) \times \frac{M(N_{\rm final}, Z_{\rm final})}{M_{\rm trial}}. \tag{4}$$

III. RESULTS AND DISCUSSION

We plot in Fig. 1 the calculated primary and final production cross sections of the TLFs with $Z = 78$–86 in the reaction ^{136}Xe + ^{208}Pb at $E_{\rm c.m.} = 450$ MeV (about $1.05V_B$, where V_B is the Bass barrier). The experimental results are taken from Ref. [15]. The predictions of GRAZING are also shown for comparisons. We note that for $Z = 78$–83, the cross sections of the neutron-rich isotopes can be well reproduced by TDHF+GEMINI while the neutron-deficient ones are underestimated. For $Z = 84$ and 85, the maxima of the distributions are close to the experimental data. However, the curves have

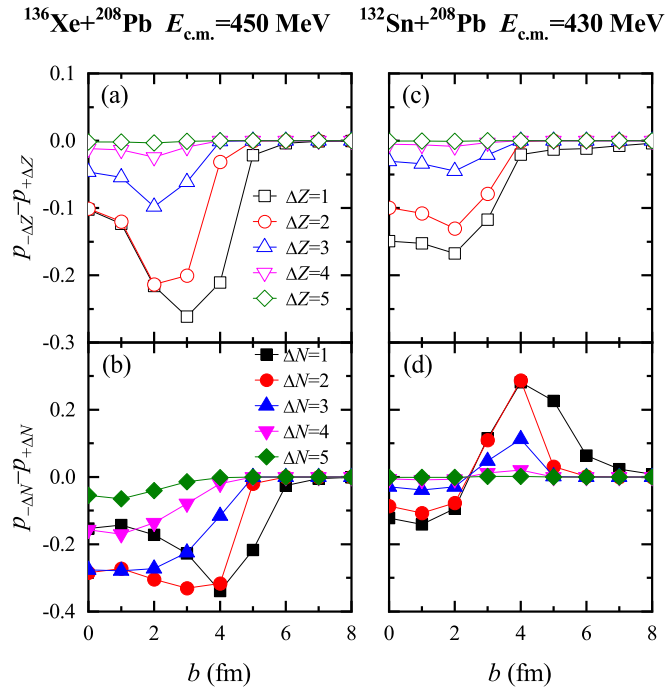

FIG. 2. Differences between the probabilities of (a) proton [(b) neutron] stripping and pickup channels as functions of the impact parameter for ^{136}Xe + ^{208}Pb at $E_{\rm c.m.} = 450$ MeV, respectively. For proton (neutron) transfer channels, the results are integrated over neutron (proton) numbers. The results of ^{132}Sn + ^{208}Pb at $E_{\rm c.m.} = 430$ MeV are shown in panels (c) and (d).

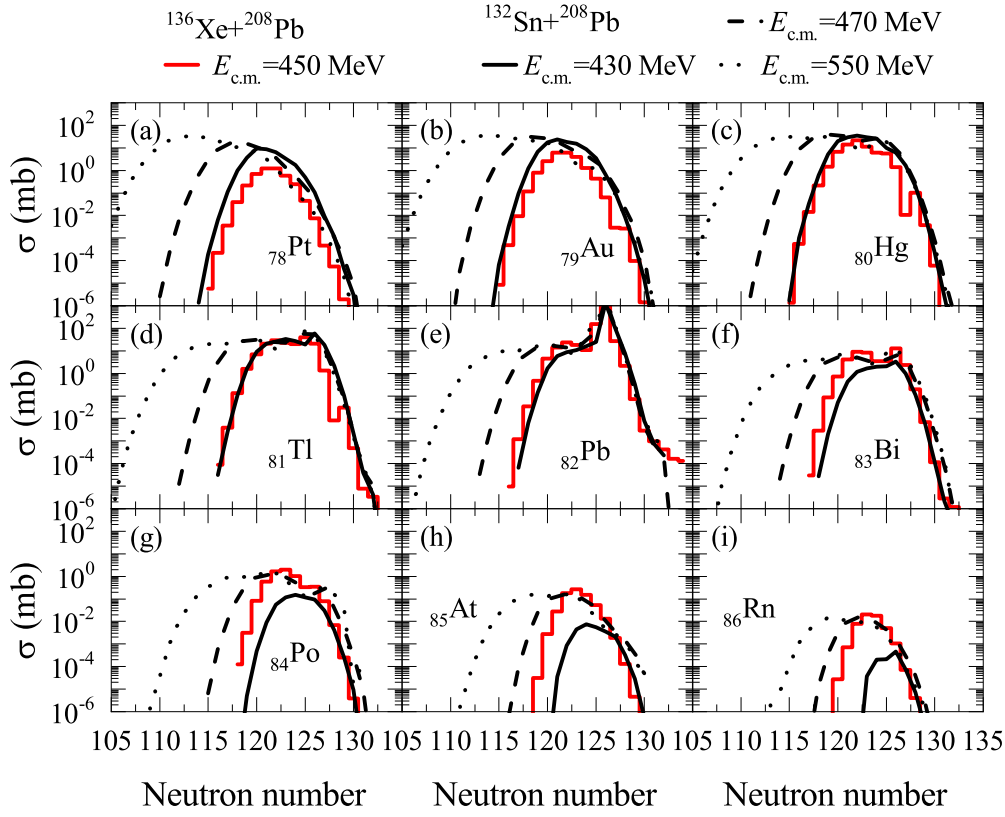

FIG. 3. Calculated production cross sections of the TLFs in ^{136}Xe + ^{208}Pb at $E_{c.m.} = 450$ MeV, which are shown as red solid folding lines. The results of ^{132}Sn + ^{208}Pb at $E_{c.m.} = 430$, 470, and 550 MeV are presented as black solid, dashed, and dotted lines, respectively.

a shift of about three neutrons to smaller N side in our model. As the number of transferred nucleons increases, the discrepancies between our predictions—both the production cross sections and the widths of the isotopic distributions—and the experimental data get larger. These isotopes far away from the entrance channel are mainly produced in deep-inelastic collisions in which violent particle exchange and large energy dissipation are involved. The underestimation in TDHF might be interpreted as the lack of two-body collisions in the pure mean-field model [79,80].

By comparing the results of GRAZING, one can find that the cross sections of the neutron-rich isotopes with $Z =$ 78–80 in GRAZING are comparable with TDHF+GEMINI results, while those of the neutron-rich ones with $Z \geqslant 81$ in GRAZING are larger. However, the cross sections of the neutron-deficient isotopes in GRAZING are orders of magnitude lower than our predictions. Another interesting point is that the de-excitation effect is much stronger in TDHF+GEMINI: About four neutrons are evaporated in the de-excitation process in TDHF+GEMINI while only one neutron is emitted in GRAZING. The above discrepancies between the two different model predictions can be easily understood since only peripheral collisions are considered in GRAZING while all impact parameters ranging from central to grazing regions are included in TDHF+GEMINI.

In Ref. [11], Zagrebaev proposed ^{132}Sn + ^{208}Pb as a better candidate to produce neutron-rich nuclei around $N = 126$. In order to check this reaction in the framework of the mean-field model, as a first step, the nucleon-transfer probabilities at different impact parameters in ^{136}Xe + ^{208}Pb and ^{132}Sn + ^{208}Pb are calculated. For ^{132}Sn + ^{208}Pb, we find that the transfer properties are similar for various incident energies even up to $2V_B$. Here we use the results of $E_{c.m.} = 430$ MeV (about $1.08V_B$) as an example. In the upper panels of Fig. 2, we present the differences between the probabilities of proton stripping ($-\Delta Z$) and pickup ($+\Delta Z$) channels. Note that the results are integrated over neutron numbers. It can be found that the proton pickup channels are favored at all impact parameters in both reactions. The differences between the probabilities of neutron stripping ($-\Delta N$) and pickup ($+\Delta N$) channels (the results are integrated over proton numbers) are plotted in the lower panels of Fig. 2. One can see that the neutron pickup channels are favored at all impact parameters for ^{136}Xe + ^{208}Pb and in $b \leqslant 2$ fm regions for ^{132}Sn + ^{208}Pb. However, a changing of the direction of neutron transfer is observed in ^{132}Sn + ^{208}Pb when $b \geqslant 3$ fm. The favored proton pickup and neutron stripping modes in ^{132}Sn + ^{208}Pb are quite beneficial for producing neutron-rich nuclei. These behaviors can be partly interpreted as the results of isospin equilibration: The N/Z values of ^{132}Sn, ^{136}Xe, and ^{208}Pb are 1.64, 1.52, and 1.54, respectively. In the dynamical process, the N/Z of the PLF and TLF should approach the values of the compound systems. This effect is also discussed in recent work of MNT reactions [32,33,55].

Figure 3 shows the calculated isotopic production cross sections of the TLFs with $Z = 78$ to $Z = 86$ in the two

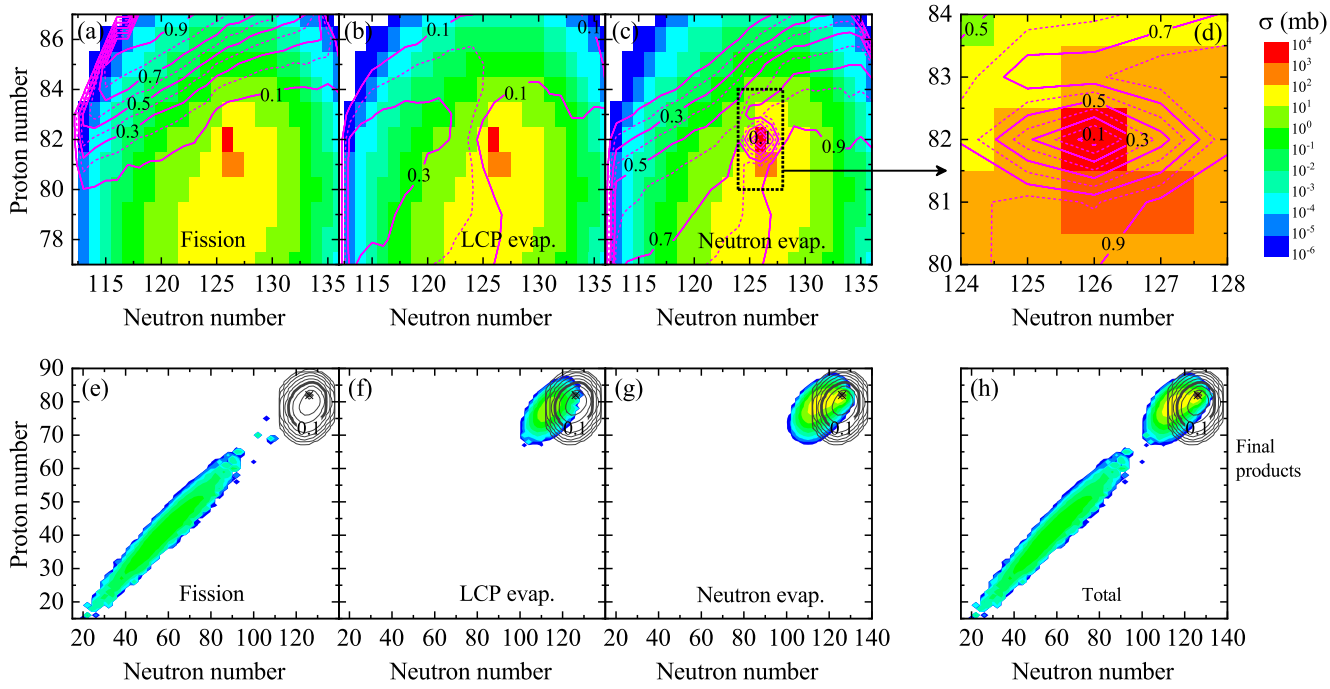

FIG. 4. Contributions of three different decay modes in the de-excitation process of the excited TLFs in ^{132}Sn + ^{208}Pb at $E_{\rm c.m.} = 550$ MeV: (a) fission of heavy nuclei (see text for details), (b) LCP emission, and (c) pure neutron evaporation. An enlargement of panel (c) for $80 \leqslant Z \leqslant 84$ and $124 \leqslant N \leqslant 128$ is presented in panel (d). The ratios η_1, η_2, and η_3 in these panels are presented as pink contour lines which are spaced by 0.1 in linear scale. The color-filled contours on a logarithmic scale in panel (a)–(d) are the primary cross sections of the TLFs. Panels (e)–(g) show the cross sections of the final products with only one of the three decay modes considered. The total cross sections of the final products are shown in panel (h). The primary cross sections of TDHF are also presented in panels (e)–(h) as solid contour lines on a logarithmic scale for comparison (the thick line is for $\sigma = 0.1$ mb). ^{208}Pb is labeled as a cross in the lower panels.

reactions. For ^{132}Sn + ^{208}Pb, three incident energies from $1.08V_B$ to $1.38V_B$ are considered. One can find that ^{132}Sn + ^{208}Pb at $E_{\rm c.m.} = 430$ MeV has the advantage over ^{136}Xe + ^{208}Pb at $E_{\rm c.m.} = 450$ MeV to produce neutron-rich isotopes with $Z \leqslant 82$. This is in accordance with the conclusion of Fig. 2. But we should note that though neutron stripping and proton pickup channels dominate in the dynamic process for all the three incident energies in ^{132}Sn + ^{208}Pb, the advantages to produce neutron-rich isotopes are not observed for $E_{\rm c.m.} =$ 470 and 550 MeV. Another interesting point is that the cross sections of neutron-rich isotopes with $Z \geqslant 79$ produced in ^{132}Sn + ^{208}Pb depend slightly on the incident energy, while the cross sections of all the neutron-deficient ones increase with the increasing incident energy, showing a very strong dependence on it. These phenomena should be related to the de-excitation process.

In order to see the de-excitation effect on the final production cross sections, the proportions of different decay modes in GEMINI++ are calculated. The decay modes of a certain primary excited fragment with (N, Z) produced after TDHF collision can be categorized into three types: (1) fission of heavy nuclei [with neutron evaporation and with or without light charged particle (LCP) emission], (2) LCP emission (with neutron evaporation but without fission), and (3) pure neutron evaporation (no fission and without LCP emission). The numbers of events for each binary decay mode are counted and denoted as $M_{\rm mode\ i}$, where $i = 1, 2, 3$ as mentioned above. The relative ratios of these modes are $\eta_i = \frac{\sigma_{\rm mode\ i}}{\sigma_{N,Z}}$, where

$$\sigma_{\rm mode\ i} = 2\pi \int_{b_{\rm min}}^{b_{\rm max}} b{\rm d}b P_{N,Z}(b) \frac{M_{\rm mode\ i}}{M_{\rm trial}} \tag{5}$$

and $\sigma_{N,Z}$ is obtained through Eq. (3).

We have calculated η_i for all the three incident energies and find that neutron evaporation dominates for $E_{\rm c.m.} = 430$ MeV while LCP emission and fission of heavy nuclei become more and more important with the increasing incident energy. To get clear insight into all these modes, the results of $E_{\rm c.m.} =$ 550 MeV are shown as pink contour lines in linear scale in Figs. 4(a)–4(d) together with the cross sections of the final products presented in Figs. 4(e)–4(h). The primary production cross sections are presented in Figs. 4(a)–4(d) as color-filled contours while in Figs. 4(e)–4(h) they are shown as black solid contour lines on a logarithmic scale. It can be found that the decay mode differs much for different isotopes. For example, $\eta_1 = 0.63$, $\eta_2 = 0.28$, and $\eta_3 = 0.09$ are observed for $Z = 84$ and $N = 118$, which means that this fragment has a probability of 0.63 to undergo fission in the de-excitation process. However, for $Z = 84$ and $N = 130$, η_1, η_2, and η_3 become 0.11, 0.09, and 0.8, respectively, indicating that neutron evaporation plays the dominant role. The final products for each de-excitation process are also different. From Fig. 4(e), one can find that if only fission process is accounted, center of

the distribution shifts toward $Z \approx 40$ and $N \approx 60$, which is far away from ^{208}Pb region. As shown in Fig. 4(f), LCP emission shifts the center of the distribution toward $Z \approx 78$ and $N \approx 114$. However, if pure neutron evaporation is accounted for, the distributions moves to a lower N region with Z unchanged.

From Fig. 4(c), one can see that neutron evaporation is dominant for almost all neutron-rich isotopes. For better visualization, we zoom in and plot the results for $80 \leqslant Z \leqslant 84$ and $124 \leqslant N \leqslant 128$ in Fig. 4(d), and one can notice that neutron evaporation is also observed for ^{208}Pb nuclei. However, this happens only for ^{208}Pb nuclei produced in deep-inelastic collisions which has minor contribution to the total cross sections of ^{208}Pb since most of them are from peripheral collisions. More neutrons will be evaporated in the de-excitation process with the increasing incident energy as expected. This effect makes the cross sections of neutron-rich isotopes at $E_{\text{c.m.}} = 550$ MeV comparable with the other two lower-energy cases and also results in much larger cross sections of the neutron-deficient isotopes. Such energy dependence of the isotopic production cross sections was also observed in Ref. [31] for $^{136}\text{Xe} + ^{208}\text{Pb}$. From Figs. 4(a) and 4(b), we note that LCP emission plays an important role for neutron-deficient nuclei with $78 \leqslant Z \leqslant 84$, and fission dominates for neutron-deficient nuclei with $Z > 82$. Recently, Yanez and Loveland made modifications to GRAZING by taking into account fission decay of the primary fragments, named GRAZING-F. This improves the final production cross sections for very heavy systems. Therefore, we suggest considering LCP emission and fission of heavy nuclei in the de-excitation process if the incident energy is much above the Coulomb barrier or if the reaction system is very heavy.

To get a deep understanding of the production mechanisms of neutron-rich nuclei in $^{132}\text{Sn} + ^{208}\text{Pb}$, as an example, in Figs. 5(a)–5(e) we present the predicted production cross sections of the TLFs in different impact parameter regions at $E_{\text{c.m.}} = 550$ MeV, with de-excitation effect included. For comparison, the results of GRAZING are also shown in Fig. 4(f). The reason for choosing this energy is that different reaction mechanisms are separated in this case. It can be found that the center of the distribution moves toward ^{208}Pb as the impact parameter increases. For $b = 8$ and 9 fm, the range of the distribution suddenly shrinks. This is because these two impact parameters are around the grazing impact parameter b_g, which is 8.6 fm based on the empirical formula [81]. It should be pointed out that the related total kinetic energy loss $E_{k,\text{loss}} = E_{\text{c.m.}} - E_k$ is smaller than 36 MeV. In this region, only a few nucleons are exchanged between the reactants and a small quantity of the collective energies is dissipated into the system. Moreover, about 50 new neutron-rich isotopes with the cross sections larger than 1 nb are observed. They are mainly from $b \leqslant 7$ fm regions where the quasifission and deep-inelastic mechanisms are dominant. The neutron-rich isotopes with $N = 126$, however, are dominantly produced in $b \geqslant 8$ partitions where deep-inelastic and quasielastic mechanisms take effect together. It is also observed that most of the neutron-deficient nuclei are from more central partitions. Our prediction of the impact parameter regions in which the neutron-rich nuclei are produced is in accordance with the recent experimental results of $^{136}\text{Xe} + ^{198}\text{Pt}$ at $E_{\text{c.m.}} =$

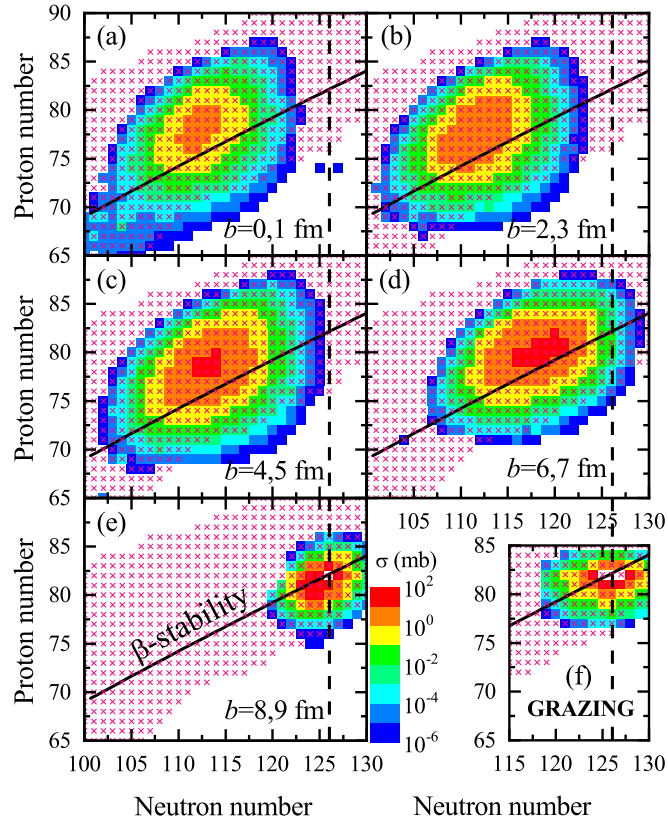

FIG. 5. (a)–(e) Predicted final production cross sections of the TLFs in $^{132}\text{Sn} + ^{208}\text{Pb}$ at $E_{\text{c.m.}} = 550$ MeV by using TDHF+GEMINI. (f) The results of GRAZING which are obtained from Ref. [78] with default parameters. The pink crosses in all the panels are known nuclei in the nuclear chart adopted from AME2016 [75,76].

689 MeV [8]. We checked the other two lower energies and note that such impact parameter regions strongly depend on the incident energy. They shift toward very central regions as the incident energy decreases. This makes it difficult to separate the reaction mechanisms apart and to determine which ones govern the production of neutron-rich nuclei. The theoretical study of $^{136}\text{Xe} + ^{208}\text{Pb}$ at $E_{\text{c.m.}} = 450$ MeV also show that heavy neutron-rich nuclei are predominantly from head-on collisions rather than peripheral collisions [11]. Therefore, the production mechanism of heavy neutron-rich nuclei in MNT reactions depends on not only the projectile-target combination but also on the incident energy. From Figs. 5(e) and 5(f), one sees that our results of $b \geqslant 8$ fm are comparable with the predictions of GRAZING. This is expected since only peripheral collisions are included in GRAZING. The exclusion of more central partitions in GRAZING results in the underestimations of neutron-deficient nuclei, as shown in Figs. 1 and 5.

IV. SUMMARY

We have performed a microscopic investigation on the transfer reactions of ^{136}Xe, $^{132}\text{Sn} + ^{208}\text{Pb}$ by a 3D TDHF approach. The production cross sections of the primary excited TLFs are calculated by using the PNP method. Furthermore,

a state-of-art statistical model, GEMINI++, is used to treat the de-excitation of the primary fragments. The results indicate that the cross sections of neutron-rich isotopes with $Z = 78$–83 in ^{136}Xe + ^{208}Pb at $E_{\mathrm{c.m.}} = 450$ MeV can be well reproduced. For larger transfer channels, there are some discrepancies between the data and model predictions which may be interpreted as a result of omission of two-body collisions in TDHF. We have applied the same method to ^{132}Sn + ^{208}Pb at three different incident energies from $1.08V_B$ to $1.38V_B$. It is found that more neutron-rich nuclei around $N = 126$ can be produced in this system due to the favored neutron stripping and proton pickup channels, but one should note that the experimental intensities of radioactive beams may be orders of magnitude lower than those with stable beams at present. Thus, the advantage of using ^{132}Sn to produce neutron-rich nuclei around $N = 126$ may be canceled. Second-generation radioactive beam facilities like the European EURISOL may shed light on this predicament, where beam intensities on the order of 10^{12} will be available for ^{132}Sn in the future [82].

A detailed analysis of the de-excitation modes in ^{132}Sn + ^{208}Pb indicates that neutron evaporation dominates in the de-excitation process. Fission decay of heavy nuclei and LCP emission are found to play important roles on the final production cross sections as the incident energy increases. They should be taken into account in the treatment of de-excitation when the incident energy is much above the barrier.

The production cross sections of the TLFs in ^{132}Sn + ^{208}Pb show a strong dependence on the impact parameter. Neutron-rich nuclei are synthesized in both quasifission and deep-inelastic collisions. Those around $N = 126$ closure, however, are mainly from peripheral (grazing) collisions.

ACKNOWLEDGMENTS

We thank Prof. H. Z. Liang for fruitful discussions. X.J. thanks P. W. Wen for helpful discussions on the GRAZING model. This work was supported by the National Natural Science Foundation of China (Projects No. 11705118, No. 11647026, and No. 11475115) and Natural Science Foundation of SZU (Grant No. 2016017).

[1] E. K. Hulet, R. W. Lougheed, J. F. Wild, J. H. Landrum, P. C. Stevenson, A. Ghiorso, J. M. Nitschke, R. J. Otto, D. J. Morrissey, P. A. Baisden, B. F. Gavin, D. Lee, R. J. Silva, M. M. Fowler, and G. T. Seaborg, Search for Superheavy Elements in the Bombardment of ^{248}Cm with ^{48}Ca, Phys. Rev. Lett. **39**, 385 (1977).

[2] H. Essel, K. Hartel, W. Henning, P. Kienle, H. J. Körner, K. E. Rehm, P. Sperr, W. Wagner, and H. Spieler, Charge and mass transfer in the reaction ^{136}Xe + ^{208}Pb at energies close to the Coulomb barrier, Z. Phys. A **289**, 265 (1979).

[3] H. Freiesleben, K. D. Hildenbrand, F. Pühlhofer, W. F. W. Schneider, R. Bock, D. v. Harrach, and H. J. Specht, The reaction ^{238}U + ^{238}U at 7.42 MeV/u, Z. Phys. A **292**, 171 (1979).

[4] M. Schädel, W. Brüchle, H. Gäggeler, J. V. Kratz, K. Sümmerer, G. Wirth, G. Herrmann, R. Stakemann, G. Tittel, N. Trautmann, J. M. Nitschke, E. K. Hulet, R. W. Lougheed, R. L. Hahn, and R. L. Ferguson, Actinide Production in Collisions of ^{238}U with ^{248}Cm, Phys. Rev. Lett. **48**, 852 (1982).

[5] K. J. Moody, D. Lee, R. B. Welch, K. E. Gregorich, G. T. Seaborg, R. W. Lougheed, and E. K. Hulet, Actinide production in reactions of heavy ions with ^{248}Cm, Phys. Rev. C **33**, 1315 (1986).

[6] R. B. Welch, K. J. Moody, K. E. Gregorich, D. Lee, and G. T. Seaborg, Dependence of actinide production on the mass number of the projectile: Xe + ^{248}Cm, Phys. Rev. C **35**, 204 (1987).

[7] H. Grawe, K. Langanke, and G. Martínez-Pinedo, Nuclear structure and astrophysics, Rep. Prog. Phys. **70**, 1525 (2007).

[8] Y. X. Watanabe, Y. H. Kim, S. C. Jeong, Y. Hirayama, N. Imai, H. Ishiyama, H. S. Jung, H. Miyatake, S. Choi, J. S. Song, E. Clement, G. de France, A. Navin, M. Rejmund, C. Schmitt, G. Pollarolo, L. Corradi, E. Fioretto, D. Montanari, M. Niikura, D. Suzuki, H. Nishibata, and J. Takatsu, Pathway for the Production of Neutron-Rich Isotopes around the $N = 126$ Shell Closure, Phys. Rev. Lett. **115**, 172503 (2015).

[9] V. Zagrebaev and W. Greiner, Shell effects in damped collisions: A new way to superheavies, J. Phys. G: Nucl. Part. Phys. **34**, 2265 (2007).

[10] V. Zagrebaev and W. Greiner, Production of New Heavy Isotopes in Low-Energy Multinucleon Transfer Reactions, Phys. Rev. Lett. **101**, 122701 (2008).

[11] V. I. Zagrebaev and W. Greiner, Production of heavy and superheavy neutron-rich nuclei in transfer reactions, Phys. Rev. C **83**, 044618 (2011).

[12] S. Heinz and O. Beliuskina, Deep inelastic transfer reactions – A new way to exotic nuclei? J. Phys.: Conf. Ser. **515**, 012007 (2014).

[13] S. Heinz, H. M. Devaraja, O. Beliuskina, V. Comas, S. Hofmann, C. Hornung, G. Münzenberg, D. Ackermann, M. Gupta, R. A. Henderson, F. P. Heßberger, B. Kindler, B. Lommel, R. Mann, J. Maurer, K. J. Moody, K. Nishio, A. G. Popeko, D. A. Shaughnessy, M. A. Stoyer, and A. V. Yeremin, Synthesis of new transuranium isotopes in multinucleon transfer reactions using a velocity filter, Eur. Phys. J. A **52**, 278 (2016).

[14] E. M. Kozulin, E. Vardaci, G. N. Knyazheva, A. A. Bogachev, S. N. Dmitriev, I. M. Itkis, M. G. Itkis, A. G. Knyazev, T. A. Loktev, K. V. Novikov, E. A. Razinkov, O. V. Rudakov, S. V. Smirnov, W. Trzaska, and V. I. Zagrebaev, Mass distributions of the system ^{136}Xe + ^{208}Pb at laboratory energies around the Coulomb barrier: A candidate reaction for the production of neutron-rich nuclei at $N = 126$, Phys. Rev. C **86**, 044611 (2012).

[15] J. S. Barrett, W. Loveland, R. Yanez, S. Zhu, A. D. Ayangeakaa, M. P. Carpenter, J. P. Greene, R. V. F. Janssens, T. Lauritsen, E. A. McCutchan, A. A. Sonzogni, C. J. Chiara, J. L. Harker, and W. B. Walters, ^{136}Xe + ^{208}Pb reaction: A test of models of multinucleon transfer reactions, Phys. Rev. C **91**, 064615 (2015).

[16] O. Beliuskina, S. Heinz, V. Zagrebaev, V. Comas, C. Heinz, S. Hofmann, R. Knöbel, M. Stahl, D. Ackermann, F. P. Heßberger,

B. Kindler, B. Lommel, J. Maurer, and R. Mann, On the synthesis of neutron-rich isotopes along the $N = 126$ shell in multinucleon transfer reactions, Eur. Phys. J. A **50**, 161 (2014).
[17] A. Winther, Grazing reactions in collisions between heavy nuclei, Nucl. Phys. A **572**, 191 (1994).
[18] A. Winther, Dissipation, polarization and fluctuation in grazing heavy-ion collisions and the boundary to the chaotic regime, Nucl. Phys. A **594**, 203 (1995).
[19] L. Corradi, A. M. Stefanini, D. Ackermann, S. Beghini, G. Montagnoli, C. Petrache, F. Scarlassara, C. H. Dasso, G. Pollarolo, and A. Winther, Multinucleon transfer reactions in $^{32}S + ^{208}Pb$ close to the Coulomb barrier, Phys. Rev. C **49**, R2875 (1994).
[20] C. H. Dasso, G. Pollarolo, and A. Winther, Systematics of Isotope Production with Radioactive Beams, Phys. Rev. Lett. **73**, 1907 (1994).
[21] L. Corradi, G. Pollarolo, and S. Szilner, Multinucleon transfer processes in heavy-ion reactions, J. Phys. G: Nucl. Part. Phys. **36**, 113101 (2009).
[22] L. Corradi, A. M. Stefanini, C. J. Lin, S. Beghini, G. Montagnoli, F. Scarlassara, G. Pollarolo, and A. Winther, Multinucleon transfer processes in $^{64}Ni + ^{238}U$, Phys. Rev. C **59**, 261 (1999).
[23] S. Szilner, L. Corradi, G. Pollarolo, S. Beghini, B. R. Behera, E. Fioretto, A. Gadea, F. Haas, A. Latina, G. Montagnoli, F. Scarlassara, A. M. Stefanini, M. Trotta, A. M. Vinodkumar, and Y. Wu, Multinucleon transfer processes in $^{40}Ca + ^{208}Pb$, Phys. Rev. C **71**, 044610 (2005).
[24] D. Montanari, L. Corradi, S. Szilner, G. Pollarolo, E. Fioretto, G. Montagnoli, F. Scarlassara, A. M. Stefanini, S. Courtin, A. Goasduff, F. Haas, D. Jelavić Malenica, C. Michelagnoli, T. Mijatović, N. Soić, C. A. Ur, and M. Varga Pajtler, Neutron Pair Transfer in $^{60}Ni + ^{116}Sn$ Far below the Coulomb Barrier, Phys. Rev. Lett. **113**, 052501 (2014).
[25] F. Galtarossa, L. Corradi, S. Szilner, E. Fioretto, G. Pollarolo, T. Mijatović, D. Montanari, D. Ackermann, D. Bourgin, S. Courtin, G. Fruet, A. Goasduff, J. Grebosz, F. Haas, D. Jelavić Malenica, S. C. Jeong, H. M. Jia, P. R. John, D. Mengoni, M. Milin, G. Montagnoli, F. Scarlassara, N. Skukan, N. Soić, A. M. Stefanini, E. Strano, V. Tokić, C. A. Ur, J. J. Valiente-Dobón, and Y. X. Watanabe, Mass correlation between light and heavy reaction products in multinucleon transfer $^{197}Au + ^{130}Te$ collisions, Phys. Rev. C **97**, 054606 (2018).
[26] T. Mijatović, S. Szilner, L. Corradi, D. Montanari, G. Pollarolo, E. Fioretto, A. Gadea, A. Goasduff, D. J. a. c. Malenica, N. Mărginean, M. Milin, G. Montagnoli, F. Scarlassara, N. Soić, A. M. Stefanini, C. A. Ur, and J. J. Valiente-Dobón, Multinucleon transfer reactions in the $^{40}Ar + ^{208}Pb$ system, Phys. Rev. C **94**, 064616 (2016).
[27] Y. Penionzhkevich, G. Adamian, and N. Antonenko, Towards neutron drip line via transfer-type reactions, Phys. Lett. B **621**, 119 (2005).
[28] G. G. Adamian, N. V. Antonenko, S. M. Lukyanov, and Y. E. Penionzhkevich, Possibility of production of neutron-rich isotopes in transfer-type reactions at intermediate energies, Phys. Rev. C **78**, 024613 (2008).
[29] G. G. Adamian, N. V. Antonenko, V. V. Sargsyan, and W. Scheid, Possibility of production of neutron-rich Zn and Ge isotopes in multinucleon transfer reactions at low energies, Phys. Rev. C **81**, 024604 (2010).
[30] G. G. Adamian, N. V. Antonenko, and D. Lacroix, Production of neutron-rich Ca, Sn, and Xe isotopes in transfer-type reactions with radioactive beams, Phys. Rev. C **82**, 064611 (2010).
[31] Z.-Q. Feng, Production of neutron-rich isotopes around $N = 126$ in multinucleon transfer reactions, Phys. Rev. C **95**, 024615 (2017).
[32] L. Zhu, J. Su, W.-J. Xie, and F.-S. Zhang, Theoretical study on production of heavy neutron-rich isotopes around the $N = 126$ shell closure in radioactive beam induced transfer reactions, Phys. Lett. B **767**, 437 (2017).
[33] X. J. Bao, S. Q. Guo, J. Q. Li, and H. F. Zhang, Influence of neutron excess of projectile on multinucleon transfer reactions, Phys. Lett. B **785**, 221 (2018).
[34] N. Wang and L. Guo, New neutron-rich isotope production in $^{154}Sm + ^{160}Gd$, Phys. Lett. B **760**, 236 (2016).
[35] H. Yao and N. Wang, Microscopic dynamics simulations of multinucleon transfer in $^{86}Kr + ^{64}Ni$ at 25 MeV/nucleon, Phys. Rev. C **95**, 014607 (2017).
[36] C. Li, P. Wen, J. Li, G. Zhang, B. Li, X. Xu, Z. Liu, S. Zhu, and F.-S. Zhang, Production mechanism of new neutron-rich heavy nuclei in the $^{136}Xe + ^{198}Pt$, Phys. Lett. B **776**, 278 (2018).
[37] A. V. Karpov and V. V. Saiko, Modeling near-barrier collisions of heavy ions based on a Langevin-type approach, Phys. Rev. C **96**, 024618 (2017).
[38] P. A. M. Dirac, Note on exchange phenomena in the Thomas atom, Math. Proc. Cambridge **26**, 376 (1930).
[39] P. Bonche, S. Koonin, and J. W. Negele, One-dimensional nuclear dynamics in the time-dependent Hartree-Fock approximation, Phys. Rev. C **13**, 1226 (1976).
[40] C. Simenel and P. Chomaz, Nonlinear vibrations in nuclei, Phys. Rev. C **68**, 024302 (2003).
[41] A. S. Umar and V. E. Oberacker, Time-dependent response calculations of nuclear resonances, Phys. Rev. C **71**, 034314 (2005).
[42] J. A. Maruhn, P. G. Reinhard, P. D. Stevenson, J. R. Stone, and M. R. Strayer, Dipole giant resonances in deformed heavy nuclei, Phys. Rev. C **71**, 064328 (2005).
[43] A. S. Umar and V. E. Oberacker, Density-constrained time-dependent Hartree-Fock calculation of $^{16}O + ^{208}Pb$ fusion cross-sections, Eur. Phys. J. A **39**, 243 (2009).
[44] C. Simenel, R. Keser, A. S. Umar, and V. E. Oberacker, Microscopic study of $^{16}O + ^{16}O$ fusion, Phys. Rev. C **88**, 024617 (2013).
[45] X. Jiang, J. A. Maruhn, and S. Yan, Microscopic study of noncentral effects in heavy-ion fusion reactions with spherical nuclei, Phys. Rev. C **90**, 064618 (2014).
[46] X. Jiang, J. A. Maruhn, and S. W. Yan, Configuration transition effect in heavy-ion fusion reactions with deformed nuclei, Europhys. Lett. **112**, 12001 (2015).
[47] A. S. Umar, V. E. Oberacker, J. A. Maruhn, and P.-G. Reinhard, Microscopic description of nuclear fission dynamics, J. Phys. G: Nucl. Part. Phys. **37**, 064037 (2010).
[48] P. Goddard, P. Stevenson, and A. Rios, Fission dynamics within time-dependent Hartree-Fock: Deformation-induced fission, Phys. Rev. C **92**, 054610 (2015).
[49] C. Simenel and A. S. Umar, Formation and dynamics of fission fragments, Phys. Rev. C **89**, 031601(R) (2014).
[50] J. A. Maruhn, P.-G. Reinhard, P. D. Stevenson, and M. R. Strayer, Spin-excitation mechanisms in Skyrme-force time-dependent Hartree-Fock calculations, Phys. Rev. C **74**, 027601 (2006).

[51] N. Loebl, A. S. Umar, J. A. Maruhn, P.-G. Reinhard, P. D. Stevenson, and V. E. Oberacker, Single-particle dissipation in a time-dependent Hartree-Fock approach studied from a phase-space perspective, Phys. Rev. C **86**, 024608 (2012).

[52] G.-F. Dai, L. Guo, E.-G. Zhao, and S.-G. Zhou, Dissipation dynamics and spin-orbit force in time-dependent Hartree-Fock theory, Phys. Rev. C **90**, 044609 (2014).

[53] L. Guo, C. Simenel, L. Shi, and C. Yu, The role of tensor force in heavy-ion fusion dynamics, Phys. Lett. B **782**, 401 (2018).

[54] K. Wen, M. C. Barton, A. Rios, and P. D. Stevenson, Two-body dissipation effect in nuclear fusion reactions, Phys. Rev. C **98**, 014603 (2018).

[55] A. S. Umar, C. Simenel, and W. Ye, Transport properties of isospin asymmetric nuclear matter using the time-dependent Hartree-Fock method, Phys. Rev. C **96**, 024625 (2017).

[56] K. Sekizawa and K. Yabana, Time-dependent Hartree-Fock calculations for multinucleon transfer processes in ^{40,48}Ca + ^{124}Sn, ^{40}Ca + ^{208}Pb, and ^{58}Ni + ^{208}Pb reactions, Phys. Rev. C **88**, 014614 (2013).

[57] K. Sekizawa and K. Yabana, Particle-number projection method in time-dependent Hartree-Fock theory: Properties of reaction products, Phys. Rev. C **90**, 064614 (2014).

[58] K. Sekizawa, Microscopic description of production cross sections including deexcitation effects, Phys. Rev. C **96**, 014615 (2017).

[59] X. Jiang and N. Wang, Production mechanism of neutron-rich nuclei around $N = 126$ in the multi-nucleon transfer reaction ^{132}Sn + ^{208}Pb, Chin. Phys. C **42**, 104105 (2018).

[60] Z. Wu and L. Guo, Microscopic studies of production cross sections in multinucleon transfer reaction ^{58}Ni + ^{124}Sn, Phys. Rev. C **100**, 014612 (2019).

[61] R. J. Charity, M. A. McMahan, G. J. Wozniak, R. J. McDonald, L. G. Moretto, D. G. Sarantites, L. G. Sobotka, G. Guarino, A. Pantaleo, L. Fiore, A. Gobbi, and K. D. Hildenbrand, Systematics of complex fragment emission in niobium-induced reactions, Nucl. Phys. A **483**, 371 (1988).

[62] https://bitbucket.org/arekfu/gemini.

[63] R. J. Charity, L. G. Sobotka, J. Cibor, K. Hagel, M. Murray, J. B. Natowitz, R. Wada, Y. El Masri, D. Fabris, G. Nebbia, G. Viesti, M. Cinausero, E. Fioretto, G. Prete, A. Wagner, and H. Xu, Emission of unstable clusters from hot Yb compound nuclei, Phys. Rev. C **63**, 024611 (2001).

[64] R. J. Charity, Systematic description of evaporation spectra for light and heavy compound nuclei, Phys. Rev. C **82**, 014610 (2010).

[65] Y. Larochelle, L. Gingras, G. C. Ball, L. Beaulieu, P. Gagné, E. Hagberg, Z. Y. He, D. Horn, R. Laforest, R. Roy, and C. St-Pierre, Isospin of intermediate mass fragments produced in peripheral, midperipheral, and central collisions from the ^{58}Ni + ^{12}C, ^{24}Mg reactions at 34.5A MeV, Phys. Rev. C **62**, 051602(R) (2000).

[66] J. X. Cheng, X. Jiang, S. W. Yan, and D. H. Zhang, The odd-even effect of ^{20}Ne fragmentation cross sections, J. Phys. G: Nucl. Part. Phys. **39**, 055104 (2012).

[67] X. Jiang and S. Yan, Effects of large mass transfer and statistical decay on ternary breakup in the reaction ^{238}U + ^{197}Au at 15A MeV, Phys. Rev. C **90**, 024612 (2014).

[68] J. W. Negele, The mean-field theory of nuclear structure and dynamics, Rev. Mod. Phys. **54**, 913 (1982).

[69] M. Bender, P.-H. Heenen, and P.-G. Reinhard, Self-consistent mean-field models for nuclear structure, Rev. Mod. Phys. **75**, 121 (2003).

[70] C. Simenel, Particle Transfer Reactions with the Time-Dependent Hartree-Fock Theory Using a Particle Number Projection Technique, Phys. Rev. Lett. **105**, 192701 (2010).

[71] J. A. Maruhn, P.-G. Reinhard, P. D. Stevenson, and A. S. Umar, The TDHF code Sky3D, Comput. Phys. Commun. **185**, 2195 (2014).

[72] E. Chabanat, P. Bonche, P. Haensel, J. Meyer, and R. Schaeffer, A Skyrme parametrization from subnuclear to neutron star densities Part II. Nuclei far from stabilities, Nucl. Phys. A **635**, 231 (1998).

[73] A. S. Umar and V. E. Oberacker, Center-of-mass motion and cross-channel coupling in the time-dependent Hartree-Fock theory, J. Phys. G: Nucl. Part. Phys. **36**, 025101 (2008).

[74] D. Mancusi, R. J. Charity, and J. Cugnon, Unified description of fission in fusion and spallation reactions, Phys. Rev. C **82**, 044610 (2010).

[75] W. Huang, G. Audi, M. Wang, F. Kondev, S. Naimi, and X. Xu, The AME2016 atomic mass evaluation (I). Evaluation of input data; and adjustment procedures, Chin. Phys. C **41**, 030002 (2017).

[76] M. Wang, G. Audi, F. Kondev, W. Huang, S. Naimi, and X. Xu, The AME2016 atomic mass evaluation (II). Tables, graphs and references, Chin. Phys. C **41**, 030003 (2017).

[77] P. Möller, A. Sierk, T. Ichikawa, and H. Sagawa, Nuclear ground-state masses and deformations: FRDM(2012), At. Data Nucl. Data Tables **109-110**, 1 (2016).

[78] http://nrv.jinr.ru/nrv/webnrv/grazing/.

[79] P. Grangé, J. Richert, G. Wolschin, and H. Weidenmüller, Influence of a collision term on finite-size one-dimensional TDHF, Nucl. Phys. A **356**, 260 (1981).

[80] K. Goeke and P. G. Reinhard, Time Dependent Hartree-Fock and Beyond, Prog. Theor. Phys. Suppl. **74**, 33 (1983).

[81] J. Wilczyński, Calculations of the critical angular momentum in the entrance reaction channel, Nucl. Phys. A **216**, 386 (1973).

[82] A. Bonaccorso and G. Prete, EURISOL: An European Isotope Separation On-Line radioactive ion beam facility, J. Phys.: Conf. Ser. **168**, 012023 (2009).